Synthetic Metals 162 (2012) 2052–2058

Contents lists available at SciVerse ScienceDirect

Synthetic Metals

journal homepage: www.elsevier.com/locate/synmet

Nanostructured layers of a new cross-linkable poly(3-hexylthiophene) in organic photovoltaic cells

Graça Brotas[a,1], Joana Farinhas[a,1], Quirina Ferreira[a,1], Jorge Morgado[a,b,2], Ana Charas[a,*,1]

[a] Instituto de Telecomunicações, Instituto Superior Técnico, P-1049-001 Lisbon, Portugal
[b] Department of Bioengineering, Instituto Superior Técnico-UTL, Av. Rovisco Pais, 1049-001 Lisbon, Portugal

ARTICLE INFO

Article history:
Received 4 August 2012
Received in revised form
24 September 2012
Accepted 7 October 2012
Available online 9 November 2012

Keywords:
Organic photovoltaic cells
Conjugated polymers
Cross-linkable polymers
P3HT

ABSTRACT

We report on the synthesis of a new cross-linkable poly(3-hexylthiophene) copolymer, P3HT-Ox10, consisting on regioregular blocks of 3-hexylthiophene and 10% molar of an oxetane-functionalized thiophene comonomer. This copolymer was used in the fabrication of organic photovoltaics (OPVs) upon combination with 1-(3-methoxycarbonyl)propyl-1-phenyl-(6,6)C_{61} (PCBM), either as blends or in bilayer structures. Bilayer devices with a nanostructured donor/acceptor interface were fabricated using a patterning process based on the phase separation in P3HT-Ox10:polystyrene blends. Columnar-grain films of cross-linked P3HT-Ox10 with diameters of ca. 140 nm were thereby obtained. These are the lowest dimensions achieved so far by this approach. Despite the modest power conversion efficiencies achieved, we believe that this easily implemented approach is very effective to prepare OPVs with well-defined morphologies.

© 2012 Elsevier B.V. All rights reserved.

1. Introduction

Poly(3-hexylthiophene) (P3HT) is certainly the most studied conjugated polymer in organic photovoltaic cells (OPVs), in particular when combined with electron-accepting fullerenes, leading to power conversion efficiencies (PCEs) that can reach 5% [1–3]. According to a recent report [4], almost six hundred papers were published between 2002 and 2010 on photovoltaic cells based on the P3HT:PCBM system, and more than one thousand dealt with properties of this system. A wide range of efficiency values has been reported, even when the authors apparently followed analogous device preparation procedures. It has been noted that a critical factor to achieve reproducible cell performance is the difficulty in controlling the details of the phase separation between the polymer and PCBM, even if the solvent, blend composition and post-treatment steps are maintained. The most efficient OPVs are those based on blends, also known as bulk heterojunction (BHJ) cells, where electron-donor and electron-acceptor domains interpenetrate at the nanoscale, providing a large interfacial area for exciton dissociation. In this structure, exciton dissociation is maximized when the size of electron-donor and electron-acceptor domains is of the order of the exciton diffusion length (estimated as ca. 3 nm in P3HT and 30 nm in PCBM [5]). The existence of pure donor and pure acceptor domains is beneficial to reduce charge recombination and ideal to create selective pathways for charges, providing such domains contact the right electrodes. BHJ cells are easily prepared by spin coating from blend solutions. However, details of film preparation and additional processing steps, such as solvent annealing [6], thermal annealing [7] and/or use of additives [8], have a strong effect on the final film morphology. This influence has been recognised as the primary cause for the above mentioned wide range of reported efficiencies for similar OPVs.

Recently, we reported on the preparation of well-defined nanostructured donor–acceptor bilayers based on cross-linked polyfluorene derivatives and PCBM [9,10]. The process involves the fabrication of columnar-grain films of the cross-linked donor polymer, on top of which PCBM is deposited by spin coating. The surface patterning of the cross-linkable conjugated polymer relies on the phase separation in blends with polystyrene. The process comprises: (i) spin coating of polymer blend solutions containing the cross-linkable conjugated polymer, an assisting polymer (polystyrene) and a photo-acid catalyst, on PEDOT:PSS-coated substrates (PEDOT:PSS is poly(3,4-ethylenedioxythiophene) doped with poly(styrene sulfonate)); (ii) selective cross-linking of the conjugated polymer film upon exposure to UV-irradiation and thermal annealing; (iii) removal of the assisting polymer by dissolution, leaving the cross-linked conjugated polymer scaffold on top of PEDOT:PSS. The phase separation between the two polymers

* Corresponding author. Tel.: +351 218418387; fax: +351 218418472.
E-mail addresses: gracabrotas@lx.it.pt (G. Brotas), joana.farinhas@lx.it.pt (J. Farinhas), quirinatf@lx.it.pt (Q. Ferreira), jorge.morgado@lx.it.pt (J. Morgado), ana.charas@lx.it.pt (A. Charas).
[1] Tel.: +351 218418387; fax: +351 218418472.
[2] Tel.: +351 218418451; fax: +351 218418472.

0379-6779/$ – see front matter © 2012 Elsevier B.V. All rights reserved.
http://dx.doi.org/10.1016/j.synthmet.2012.10.007

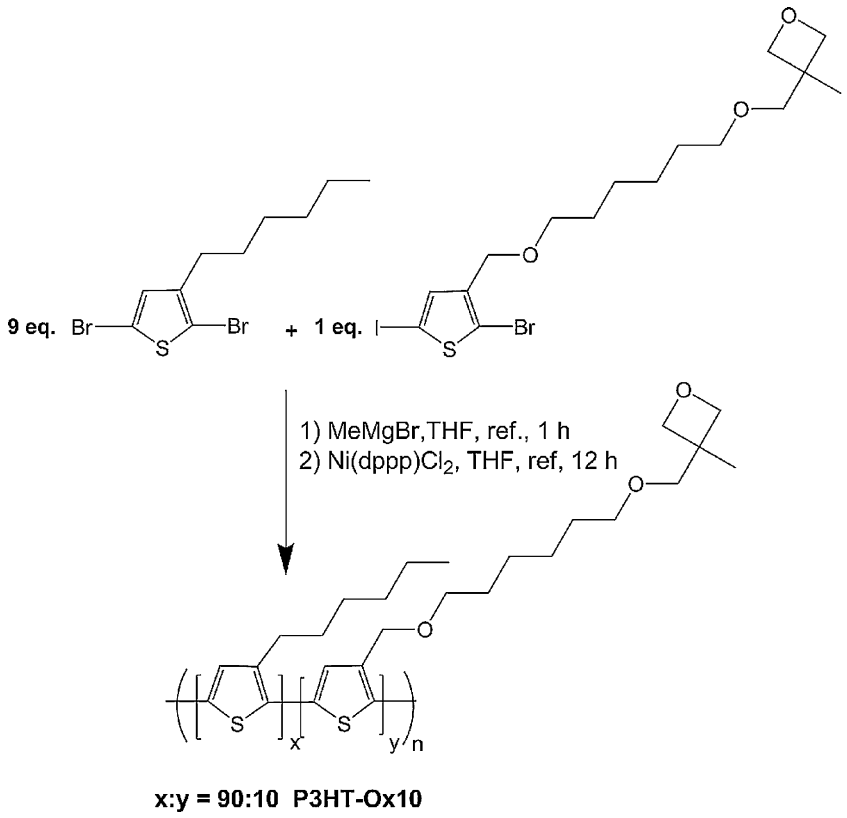

Scheme 1. Polymerization route for P3HT-Ox10.

leads to morphologies that are tuneable by the blend characteristics and the spinning speed. This patterning method provides practical advantages, as it utilizes solution techniques (spin coating) and the resulting polymer network is insoluble, therefore enabling the deposition of the electron-acceptor on top from solution. Moreover, as the electron-donor patterned film is produced in a first step, by imaging this film, we gain access to the donor–acceptor interface morphology that is formed upon deposition of the electron-acceptor material, this being a remarkable advantage when comparing with cells based on blends. Cells with well-defined donor–acceptor interfaces can also be useful to investigate the relation between morphology and cell performance and possibly to assess the relative importance of the various operation steps. Furthermore, the use of cross-linkable conjugated polymers in OPVs should afford more stable morphologies, due to the formation of insoluble polymer networks. This patterning process was developed for cross-linkable polymers derived from poly(9,9-dioctylfluorene-*alt*-bithiophene) (F8T2), bearing oxetane-containing side groups. Oxetanes react via a cationic ring-opening mechanism (CROM), leading to insoluble polymer networks. We use the {4-[(2-hydroxytetradecyl)-oxyl]-phenyl}-phenyliodonium hexafluoroantimonate photo-acid (Sigma–Aldrich) to initiate the polymerization of the oxetane side groups. Using this patterning process, we were able to obtain columnar-grain films, with columns reaching a minimum diameter of ca. 250 nm. However, this is a far too large value when comparing with the exciton diffusion length of ca. 10 nm estimated for conjugated polymers [9,10]. Efforts have been focused on the synthesis of new cross-linkable polymers, bearing oxetane functional groups, which could lead to better performing OPVs and, simultaneously, allow us to obtain patterns of smaller dimensions. Here, we report on our recent studies on a new oxetane-functionalized P3HT (P3HT-Ox10). This was synthesized as a statistical copolymer, containing only 10% molar of an oxetane-functionalized thiophene comonomer (Scheme 1). Blocks of 3-hexylthiophene in P3HT-Ox10 have a high regioregularity, in the head-to-tail configuration, according to ^{1}H NMR results. For comparison, we have also prepared the regioregular homopolymer, rr-P3HT, using the same polymerization conditions. We note that only few cross-linkable P3HTs have been reported [11–14] and, to the best of our knowledge, only one (P3HT-Br) combines both a low content in cross-linkable units (6-bromo-3-hexylthiophene) and a high regioregularity of the 3-hexylthiophene-based blocks [14].

We were able to prepare columnar-grain films of cross-linked P3HT-Ox10 with column diameters as low as 140 nm, which is roughly half the lowest dimension obtained with the cross-linkable F8T2 [9,10]. The optical and electrochemical properties of the new polymer in the pristine and cross-linked forms were investigated. Planar bilayer and BHJ cells of the new polymer combined with PCBM as electron-acceptor were also fabricated and characterized.

2. Experimental

2.1. Synthesis of P3HT-Ox10

P3HT-Ox10 was prepared from a mixture of 2,5-dibromo-3-hexylthiophene (synthesized according to ref. 15) and 10% mol of a new oxetane-functionalized monomer, following the Grignard metathesis method (GRIM) [15], in order to obtain regioregular 3-hexylthiophene blocks in the head-to-tail configuration (Scheme 1). Full details of the synthesis will be published elsewhere. For the polymerization reaction, a flask equipped with a stirring bar and a reflux condenser with a nitrogen inlet was charged with the monomers and dry THF. A 1.0 M solution of methylmagnesium bromide (MeMgBr) (Sigma–Aldrich) (1 equiv. with respect to the monomers) was added. The mixture was heated to reflux for 1 h and then cooled to room temperature. Ni(dppp)Cl_2 (Sigma–Aldrich) (0.34% mol) was added and the

mixture was stirred under reflux overnight. The mixture was poured into methanol under stirring and the precipitate was filtered into a Soxhlet thimble and extracted with methanol, hexane and chloroform. The chloroform fraction was retained and dried under reduced pressure. The homopolymer, P3HT, was also prepared and purified similarly. Both polymers, P3HT-Ox10 and P3HT, were obtained as brown-reddish solids and stored under nitrogen.

2.2. Characterization techniques

NMR spectra were recorded in a Bruker "Advance II" spectrometer (300 MHz or 400 MHz) in $CDCl_3$ with tetramethylsilane as internal reference. Number average (M_n) and weight average (M_w) molecular weights were estimated by gel permeation chromatography (GPC) in a Waters 1515 chromatograph equipped with three Styragel columns (HR5E, HR4, HR3) in series and with a Waters 2414 Differential Refractometer, using polystyrene standards (Sigma–Aldrich). GPC analyses were performed on filtered tetrahydrofuran (THF) solutions (0.2 μm, Millipore Millex HV). UV/vis absorption spectra were recorded in a Cecil 7200 spectrophotometer. The optical energy gap of the polymers was estimated from the onset of UV–vis absorption spectra recorded for spin cast films. Ionisation potentials (I_p) and electron affinities (EA) were estimated from cyclic voltammetry (CV) measurements, performed with a Solartron potentiostat and using tetrabutylammonium tetrafluoroborate (Sigma–Aldrich) in CH_3CN as the supporting electrolyte, at a scan rate of 50 mV/s. A saturated calomel reference electrode (SCE) calibrated against ferrocene, Fc/Fc^+ (0.42 V), a platinum wire as counter electrode, and a platinum disk as working electrode were used. The polymers were deposited on the working electrode by drop cast from THF solutions. As the energy level of Fc/Fc^+ is 4.8 eV below the vacuum level [16], we calculate I_p (eV) = ($E_{onset,ox}$ (V) + 4.38) and EA (eV) = ($E_{onset,red}$ (V) + 4.38). Atomic force microscopy (AFM) studies were performed on a Molecular Imaging (model 5100) system operating in non-contact mode (at a resonance frequency between 200 and 400 kHz) using silicon probes with tip radii lower than 10 nm. All images were taken with 256 × 256 pixels resolution and were processed using the same levelling procedure. Gwyddion (version 2.26) software was used to process the images. Thicknesses of the OPVs active layers were measured using a profilometer (Stylus Profilometer, DekTak 6M).

2.3. Cross-linking procedure

Toluene solutions of P3HT-Ox10 containing 4% (by weight, relative to the polymer) of the {4-[(2-hydroxytetradecyl)-oxyl]-phenyl}-phenyliodonium hexafluoroantimonate photo-acid generator (PAG) were deposited by spin coating on quartz substrates. The films were placed on a hot plate at 125 °C and illuminated with UV-light (254 nm) from a hand-held lamp (4 W) for 1 min. They were further annealed at 125 °C for 10 min in the dark. Afterwards, the films were rinsed twice with THF to remove non-cross-linked polymer chains and PAG residues.

2.4. Solar cell fabrication

OPVs were prepared on glass/ITO substrates coated with PEDOT:PSS (Heraeus Clevios P VP.AI 4083). Three different device architectures were prepared: P3HT-Ox10/PCBM nanostructured bilayer, P3HT-Ox10/PCBM planar bilayer, and polymer:PCBM BHJs.

After the deposition of the active layer (as described below), the substrates were transferred to a nitrogen-filled glove box and a thin layer of LiF (1.5 nm) and a capping layer of aluminium (ca. 100 nm) were thermally evaporated on top through a shadow mask, at a base pressure below 3×10^{-6} mbar, defining OPV active areas of 0.16 cm^2. Current–voltage (I–V) characteristics were measured under inert atmosphere (N_2) using a K2400 SourceMeter. Power conversion efficiencies (PCEs) were calculated using a solar simulator (Oriel instruments 92250A-1000) with simulated AM 1.5 G illumination at 60 mW/cm^2. The light intensity was measured with a calibrated solar cell. External quantum efficiency (EQE) spectra was determined under short-circuit conditions, using a homemade system with a Xe lamp as light source.

2.4.1. P3HT-Ox10/PCBM nanostructured bilayer

A filtered (0.45 μm pore size PTFE filter) toluene solution, containing monodisperse polystyrene (PS) (M_n = 4000, GPC standard, Aldrich), P3HT-Ox10 (1:1, w/w, total concentration of polymers = 15 mg/ml), and a catalytic amount of PAG in THF, was deposited by spin coating at 1800 rpm for 45 s on PEDOT:PSS (ca. 70 nm thick)-coated glass/ITO substrates. The films were submitted to the cross-linking protocol and imaged by Atomic Force Microscopy (AFM). The complete PS removal was confirmed by the disappearance of PS absorption bands in the infrared absorption spectrum (3030–3090 cm^{-1}). Deposition of 1-(3-methoxycarbonyl)propyl-1-phenyl-(6,6)C_{61} (PCBM) (Sigma–Aldrich) by spin coating from a chlorobenzene solution on top completed the OPV active layer fabrication.

2.4.2. P3HT-Ox10/PCBM planar bilayer

A solution of P3HT-Ox10 (20 mg/ml) in chlorobenzene and a catalytic amount of PAG in THF was stirred at 75 °C for 2 h and then spin cast (1800 rpm, 45 s) on glass/ITO/PEDOT:PSS substrates. The substrates were then submitted to the cross-linking protocol and PCBM was spin cast on top from a chlorobenzene solution (20 mg/ml).

2.4.3. Polymer:PCBM BHJs

The polymer (either P3HT or P3HT-Ox10) and PCBM were mixed in chlorobenzene (1:1, w/w, 20 mg in total/ml) and the solution was stirred at 75 °C (on a hot plate) for 2 h. Such blends solutions were spin coated (1000 rpm for 45 s) onto glass/ITO/PEDOT:PSS substrates. In the case of P3HT-Ox10:PCBM blends, in addition to such "as spun" films, cross-linked films were also prepared using the above described cross-linking protocol, in which case a catalytic amount of PAG in THF was added to the chlorobenzene solution prior to the deposition. We note that a similar amount of THF was added to the solution of P3HT-Ox10:PCBM used to fabricate the "as spun" films, in order to maintain the same solvent composition and solids concentration.

3. Results and discussion

3.1. Polymer synthesis

P3HT-Ox10 and rr-P3HT were obtained with M_n = 13,500 (PD = 1.40) and M_n = 13,200 (PD = 1.29), respectively (Table 1). Fig. 1 compares the ^1H NMR spectrum of P3HT-Ox10 with that of rr-P3HT. The peak at 6.98 ppm in the spectrum of rr-P3HT is assigned to the aromatic ^1H in 3-hexylthiophene arranged in a head-to-tail (HT-HT) configuration [17].

The NMR spectrum of P3HT-Ox10 shows also a well-defined peak at that chemical shift (6.98 ppm), indicating that the blocks of 3-hexylthiophene are highly regioregular (with the same HT-HT configuration), and two further peaks in the aromatic region, at 7.16 and 7.06 ppm. According to NMR Heteronuclear Multiple Bond Correlation (^1H, ^{13}C-HMBC) experiments, the peak at 7.16 ppm corresponds to the aromatic ^1H in the oxetane-functionalized thienyl unit whereas the peak at 7.06 ppm corresponds also to aromatic ^1H in 3-hexylthiophene units, these being probably directly linked to an oxetane-functionalized monomer. The region between

Table 1
Properties of P3HT-Ox10 and rr-P3HT.

Polymer	M_n (kDa)	PDI	$\lambda_{max,\ soln.}$ (nm)	$\lambda_{max,\ film.}$ (nm)	Eg_{opt} (eV)	$E_{ox,onset}$ (eV)	$E_{red,onset}$ (eV)	I_p (eV)	EA (eV)
rr-P3HT	13.2	1.29	446	554	1.86	0.55	−1.93	4.93	2.45
P3HT-Ox10	13.5	1.40	443	553	1.86	0.50	−1.73	4.88	2.65
Cross-linked P3HT-Ox10				503	1.89	0.74	−1.73	5.12	2.65

3.43 and 4.59 ppm is assigned to six protons in the acyclic ether groups (—CH_2O—) in the lateral chain of the oxetane-functionalized monomers. From the relative area of the peaks within this region and the peak at 2.80 ppm (this corresponding to ^1H in the —CH_2— group directly linked to the thiophene ring in 3-hexylthiophene) we determine that the cross-linkable monomer content is approximately 10% mol, i.e., the same as the molar feed ratio in the polymerization reaction.

3.2. Optical properties

The absorption spectra of both polymers, rr-P3HT and P3HT-Ox10, were determined in dilute solution and as spin casted films. In addition, films of cross-linked P3HT-Ox10 were also characterized. The solution spectra of rr-P3HT and P3HT-Ox10 in chloroform nearly overlap, with a small difference in the wavelength at maximum absorption, 446 nm for rr-P3HT and 443 nm for P3HT-Ox10 (Table 1). When going to films spin casted from toluene solutions, we find that the absorption of both polymers is red-shifted with respect to solution, with maxima at 554 nm for rr-P3HT and 553 nm for P3HT-Ox10, this shift being attributed mostly to extended conjugation length and/or interchain interactions in solid state. The absorption spectra of P3HT-Ox10 and rr-P3HT films are very similar, with identical optical gap (1.86 eV) and both showing a vibronic shoulder at about 600 nm, whose intensity has been correlated with high crystallization or chain ordering in rr-P3HT [2] (Fig. 2). This indicates that the presence of oxetane-functionalized monomers in 10% content in P3HT-Ox10 does not significantly disturb the chain ordering in the films when comparing with rr-P3HT. We observe also that if P3HT-Ox10 films are prepared from solutions containing a catalytic amount of PAG, their absorption spectrum undergoes a small blue-shift (λ_{max} = 546 nm), but the vibronic shoulder at ca. 600 nm is maintained (spectrum "P3HT-Ox10 + PAG" in Fig. 2).

As shown in Fig. 2, there is a significant reduction in intensity and a small blue-shift of the absorption spectrum of P3HT-Ox10 upon cross-linking. We conclude that a high cross-linking yield was attained on these films, since no colouration of the washing solvent (see Section 2.3) was noticed. The blue-shift of the absorption spectrum is attributed to increased disorder of the polymer backbone brought about by the cross-linking process. To investigate possible causes of the absorption decrease upon cross-linking, we have separately studied the effect of each one of the conditions used in the cross-linking protocol (addition of photo-acid, exposure to UV light, and thermal annealing). We found that none of these conditions leads, by itself, to a reduction in absorption. We therefore conclude that the observed reduction in absorption intensity is related to structural effects resulting from the cross-linking reaction. Nevertheless, it is worth noting that the absorption spectrum of P3HT-Ox10:PCBM blends does not suffer any significant change upon cross-linking, which indicates that the structural effects responsible for the optical absorption reduction are suppressed when the polymer is blended with PCBM.

3.3. Electrochemical properties

The electrochemical properties of P3HT-Ox10, both in the soluble and cross-linked forms, were investigated by cyclic voltammetry on films drop-casted on a platinum electrode. We observed that p-doping/dedoping processes at positive potentials and n-doping/dedoping at negative potentials are not completely reversible. Therefore, we carried out oxidation and reduction processes separately in fresh films. We estimate I_p and EA from the onset of oxidation and reduction potentials ($E_{onset,ox}$, $E_{onset,red}$), respectively (see Table 1). For P3HT-Ox10, we obtain I_p = 4.88 eV, which is close to the value found for rr-P3HT under the same conditions (Table 1), and EA = 2.65 eV (0.20 eV lower than that of rr-P3HT). Upon cross-linking, the I_p of P3HT-Ox10 increases by 0.24 eV (to 5.12 eV) whereas EA remains unchanged. The increase of I_p (corresponding to a lowering of the HOMO energy) is reflected in a larger optical gap and is consistent with the above mentioned detrimental effects of the cross-linking process on the π-conjugation extent.

3.4. Applications in OPVs

The nanostructured layers of cross-linked P3HT-Ox10 exhibit a columnar-grain morphology type, whose average dimensions

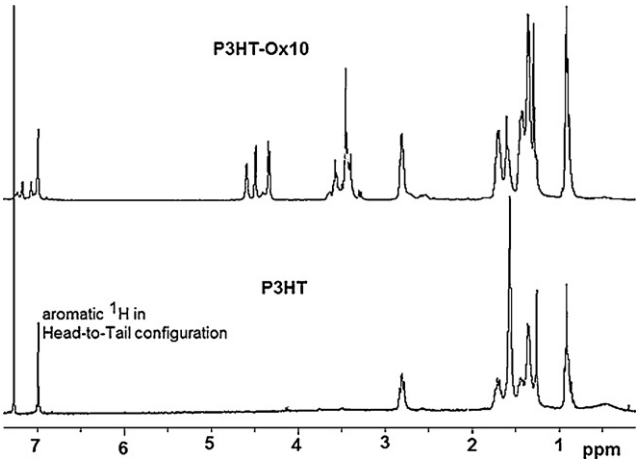

Fig. 1. ^1H NMR (300 MHz, $CDCl_3$) spectra of P3HT-Ox10 and rr-P3HT.

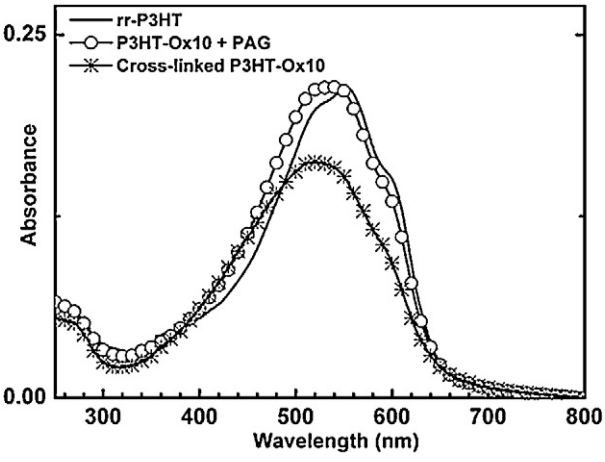

Fig. 2. UV–visible absorption spectra of rr-P3HT and P3HT-Ox10 films (in the soluble and cross-linked forms).

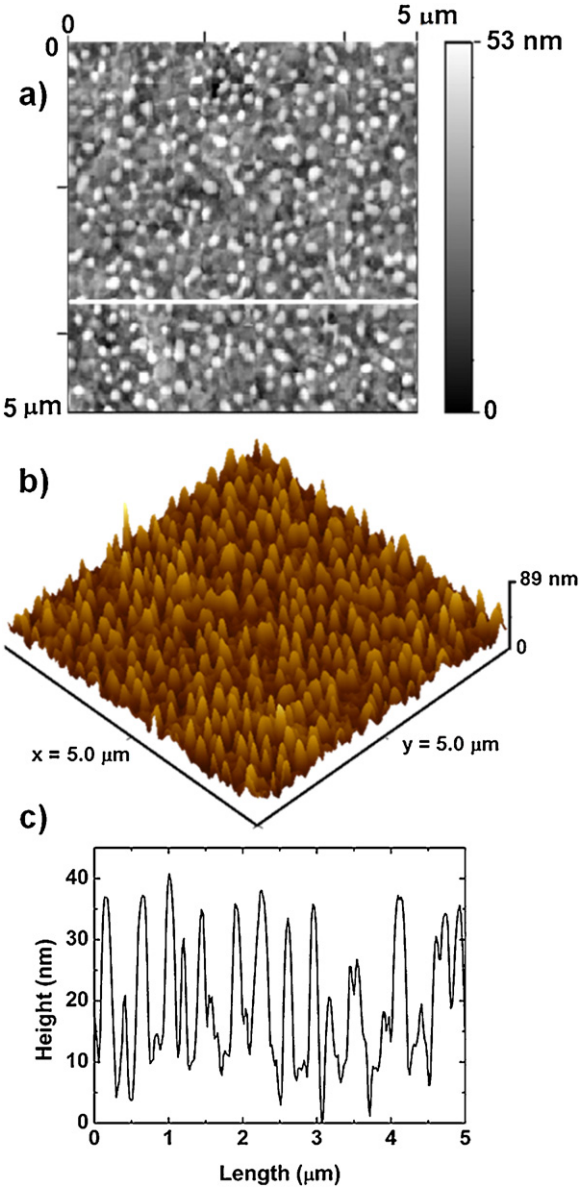

Fig. 3. (a) AFM topographic image (5 μm × 5 μm) (top image) and (b) corresponding 3D projection showing a columnar structured film of cross-linked P3HT-Ox10; (c) sectional view along a line in the AFM image.

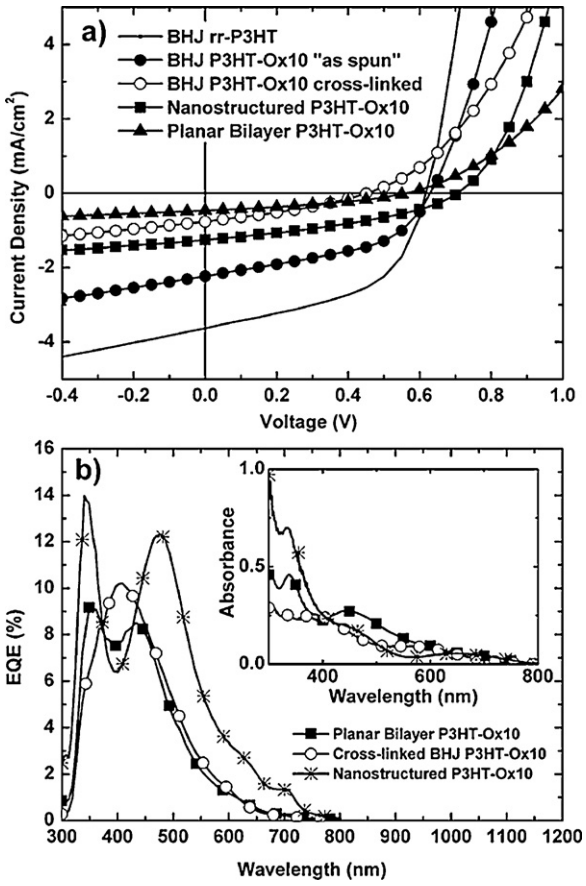

Fig. 4. (a) Current density–voltage (*J*–*V*) curves under illumination for the various OPVs, (b) External quantum efficiency (EQE) for P3HT-Ox10-based devices. The inset of (b) shows their absorption spectra.

are: column height: ~24 nm; column radius: ~70 nm and underlayer thickness (polymer layer sustaining the columnar structure): ~34 nm. Fig. 3 shows an AFM topography image (5 μm × 5 μm), its corresponding 3D projection for better visualization, and a sectional view along a line.

The dimensions of the structured films are larger than those considered ideal for the donor layer, both in terms of column radius and the underlayer thickness: these should be lower than the exciton diffusion length within the polymer (ca. 10 nm). It is worth pointing out, however, that the achieved dimensions are significantly smaller than those previously obtained, by the same procedure, for a cross-linkable poly(9,9-dioctylfluorene-*alt*-bithiophene)s [9]. PCBM was deposited, by spin coating, on top of the P3HT-Ox10 nanostructured layer and the surface was characterized by AFM. The phase images are consistent with a single material being present at the surface, indicating that PCBM completely covers the polymer film. The presence of both a PCBM layer at the cathode interface (LiF/Al) and a polymer underlayer at the anode interface (PEDOT:PSS) are beneficial for device performance, as they suppress direct percolation paths (shunts) between both electrodes. The final average thickness of the donor/acceptor bilayer was measured with a profilometer after depositing the LiF/Al layer. We then subtracted the thicknesses of the PEDOT:PSS layer plus that of LiF/Al layer and obtained ca. 110 nm for the bilayer thickness. This value should be affected by an error of ca. ±20 nm, due to the non-flat topography of the PCBM and Al surfaces, which roughly follows the pattern of the nanostructured polymer film underneath. Therefore, a layer of ca. 50 ± 20 nm of PCBM is estimated to separate the top of the columnar nanostructured polymer layer from the cathode. For comparison, planar bilayer cells with cross-linked P3HT-Ox10 and PCBM, and BHJ cells prepared with P3HT-Ox10:PCBM blends, both "as spun" and cross-linked, were also fabricated. Films of P3HT-Ox10:PCBM blends that were cross-linked and used in cells fabrication were rinsed with chlorobenzene after cell measurements. By determining the absorption of the remaining film, we estimate that ca. 75% of the polymer is retained (while PCBM is washed out) confirming a high cross-linking yield. Cells based on blends of rr-P3HT and PCBM were also prepared and tested without any annealing process ("as spun"). Fig. 4 shows the current density (*J*)–Voltage (*V*) curves recorded for the various OPVs under illumination and the External Quantum Efficiency spectra for the cells with the cross-linked polymer with different active layer structures. Table 2 summarizes the corresponding cell characteristics.

The performance of the BHJ cells based on rr-P3HT is significantly better than that reported for "as spun" cells, i.e., without any further optimization treatment, by Chen et al. [2]. These authors reported J_{SC} = 3.53 mA/cm^2, V_{OC} = 0.50 V, FF = 35%, PCE = 0.61% for OPVs based on 1:1, w/w rr-P3HT:PCBM blend prepared under the

Table 2
Performance parameters (open circuit voltage, V_{OC}, short-circuit current density, J_{SC}, fill factor, FF, and power conversion efficiency, PCE) of the OPVs studied in this work. Thicknesses of the active layers (polymer and PCBM) are also shown.

PV cell architecture	Thickness (nm)	J_{SC} (mA/cm^2)	V_{OC} (V)	FF (%)	PCE (%)
P3HT:PCBM, 1:1, BHJ	100	3.63	0.62	51	1.87
P3HT-Ox10:PCBM, 1:1, "as spun" BHJ	90	2.23	0.63	46	1.07
P3HT-Ox10:PCBM 1:1, "cross-linked" BHJ	90	0.76	0.45	32	0.18
P3HT-Ox10/PCBM, "cross-linked" planar bilayer	90	0.47	0.56	35	0.16
P3HT-Ox10/PCBM, nanostructured bilayer	110	1.25	0.71	37	0.56

Table 3
Effect of 40 min exposure to AM 1.5G illumination on the performance parameters of OPVs whose characteristics are shown in Table 2.

PV cell architecture	J_{SC} (mA/cm^2)	V_{OC} (V)	FF (%)	PCE (%)
P3HT:PCBM, 1:1, BHJ	3.48	0.60	50	1.70
P3HT-Ox10:PCBM, 1:1, "as spun" BHJ	2.07	0.62	43	0.89
P3HT-Ox10:PCBM 1:1, "cross-linked" BHJ	0.77	0.48	31	0.19
P3HT-Ox10/PCBM, planar bilayer	0.56	0.55	39	0.20

same conditions (solution concentration and solvent) though using rr-P3HT with higher molecular weight (M_w = 42,400, M_n = 21200). Although these are not the conditions yielding the most efficient P3HT-based devices, this is the report we found to closely match the device preparation conditions we used in this work. As mentioned above, various processes may be applied to optimize cell's PCE. This work is not focused in such optimization procedures. We note that the BHJ cells based on rr-P3HT, whose results are shown in Table 2, were prepared with blend solutions to which a small amount of THF had been added, to allow a better comparison with the blends prepared with P3HT-Ox10. Yet, cells prepared from solutions of rr-P3HT:PCBM blends without THF showed PCE values above 1.5%.

"As spun" P3HT-Ox10:PCBM BHJ cells showed similar V_{OC} but smaller PCE and short-circuit current than the cells based on rr-P3HT. AFM topographic and phase images of the blends based on either rr-P3HT or P3HT-Ox10 and PCBM were similar and did not reveal a noticeable phase separation between the two components nor the presence of large aggregates.

Cross-linking of the P3HT-Ox10:PCBM blends has a significant detrimental effect on cells performance. Besides the decrease of V_{OC} from 0.63 V to 0.45 V, both short-circuit current and PCE significantly decrease with respect to the "as spun" cells. Such detrimental effects should be related to structural changes and/or to the presence of ionic species produced during the cross-linking process, which may contribute to energy losses in the cell. We have previously reported, for a cross-linkable F8T2 [18], that cross-linking has a detrimental effect on the hole mobility. We believe that a similar effect is likely to occur in this case. We further note that the absorption spectrum intensity of P3HT-Ox10:PCBM blends is not significantly affected by the cross-linking process (in contrast with the films of pure polymer either from toluene or chlorobenzene solutions, as shown in Fig. 2). Therefore, the observed detrimental effect in cell performance should not be related with absorption losses.

Preliminary studies on cells stability upon exposure to continuous illumination with the solar simulator for 40 min demonstrated that BHJ and planar bilayers cells with cross-linked P3HT-Ox10 are the most stable ones among the series of tested devices. For these cells, measurements performed on the same pixels did not show any decrease in current density nor in PCE values, while the "as spun" BHJ cells based on either P3HT and soluble P3HT-Ox10 showed a decrease in the PCE values of ca. 9% and 16%, respectively (Table 3).

Surprisingly, the efficiency of the cells based on cross-linked P3HT-Ox10:PCBM blends is similar to that of the bilayer device based on cross-linked P3HT-Ox10, in spite of the much lower donor/acceptor interfacial area obtained with these planar bilayer structures. For the nanostructured cells, we find a significant performance improvement, with an increase of all performance parameters, as shown in Table 2. Yet, these cells exhibit lower values of current and efficiency than those based on the "as spun" blends.

The V_{OC} of the BHJ cells based on P3HT (0.62 V) are similar to those based on soluble P3HT-Ox10 (0.63 V), as shown in Table 2, and also similar to those typically found for the rr-P3HT:PCBM system (0.50–0.65 V) [1–4]. There is a significant decrease in V_{OC} upon cross-linking of the P3HT-Ox10:PCBM blends, leading to the lowest value (0.45 V) among the series. Although there is still an open debate on the parameters that determine the V_{OC} in organic PV cells [19–21], it is generally accepted that the theoretical upper limit is related to the difference between the highest occupied molecular orbital (HOMO) of the donor material and the lowest unoccupied molecular orbital (LUMO) of the acceptor material. The decrease of V_{OC} upon cross-linking is possibly related to interfacial effects between cross-linked P3HT-Ox10 and PCBM. We note that, as a result of the ring opening polymerization of the oxetane groups, reactive oxonium (RO^+R') species are likely to remain in P3HT-Ox10 domains. A similar effect may explain the intermediate value of V_{OC} (0.56 V) obtained for the planar bilayer device, pointing to a lower effect or lower surface concentration of such cationic groups at the interface. In contrast, V_{OC} of the bilayer devices with nanostructured interfaces (0.71 V) is even higher than that of the "as spun" BHJ cells. In this case, the films of cross-linked P3HT-OX10 are washed with THF prior to the PCBM deposition, and THF may annihilate those oxonium groups, as suggested by Müller et al. [22]. However, the reason for the higher V_{OC} is still unclear. It should be mentioned that Kim et al. [23] also found a considerably higher value (0.78 eV) for cells based on nanoimprinted layers of P3HT and PCBM spin cast on top. Other authors [24] found the same trend (increase of V_{OC} in nanoimprinted devices relative to flat bilayer devices) in pentacene-C60 systems. Another hypothesis is that the higher V_{OC} in nanostructured cells may be related to the polymer/PCBM ratio at the donor/acceptor interface and consequent effects on the polymer HOMO level and/or energy level alignment at the interface. In fact, it was demonstrated that the polymer:PCBM ratio significantly affects the V_{OC} values in P3HT:PCBM BHJ cells [25].

Concerning the variation of the fill factor, the devices with cross-linked P3HT-Ox10 show the lowest values, which may be associated to a decrease of charge mobility in cross-linked networks. Still, among such cells, the nanostructured ones exhibit the higher FF, indicating a more adequate morphology for PV operation.

The EQE spectra (Fig. 4b) show a higher contribution to the photocurrent of the polymer relative to PCBM both in the nanostructured device and in the planar bilayer cell. Due to the contribution of PCBM, the absorption spectra are blue shifted when comparing with the absorption spectrum of the polymer (Fig. 2). The EQE spectra of the planar bilayer and BHJ closely follow the corresponding absorption spectra, whereas the EQE for the

nanostructured cell shows comparable contributions of both components (polymer and PCBM) despite the lower polymer content (as indicated by its absorption spectrum).

Overall, although the morphological characteristics of the nanostructured films are still distant from the ideal ones, these results are encouraging in terms of the potential of this fabrication process. Work is currently in progress to achieve that goal.

4. Conclusions

To conclude, a new cross-linkable P3HT derivative was prepared, combining regioregular head-to-tail 3-hexylthiophene blocks with only 10% of a cross-linkable comonomer. We observe that the optical and electrochemical properties of the cross-linkable polymer are analogous to those of rr-P3HT, although a noticeable decrease in absorption of P3HT-Ox10 films is observed upon cross-linking. The new polymer was used to fabricate OPVs with a nanostructured donor/acceptor interface, utilizing a low cost, solution-based method, allowing the PCBM deposition from solution on top. The obtained columnar-grain morphology resembles the optimal architecture-type for OPV operation, since well-defined domains of the electron-donor are formed perpendicular to the cell substrate. The dimensions achieved for the columnar structures (diameters of ca. 140 nm) are the lowest fabricated by the patterning process based on the phase separation from blends of cross-linkable polymers, this representing a step forward to obtain ideal cell morphologies from such polymers. In addition, this type of structures potentially provides a platform to investigate the role of various parameters affecting OPVs performance, such as the effect of domain size. In spite of the progress achieved with respect to previous studies on similar nanostructured devices [9,10], the cells prepared with the new polymer, either BHJ or comprising nanostructured layers, still exhibit lower performance than reference BHJ cells with rr-P3HT.

Acknowledgments

The authors thank the National NMR Network IST-UTL (contract REDE/1517/RMN/2005, POCI 2010 and FCT). All the research work was supported by grants from Fundação para a Ciência e Tecnologia (FCT, Portugal) (contracts SFRH/BPD/75338/2010 SFRH/BD/62130/2009 and SFRH/BD/75221/2010) and by FCT funded projects (PTDC/CTM/101627/2008, PTDC/CTM/111263/2009, and PEst-OE/EEI/LA0008/2011)

References

[1] M. Reyes-Reyes, K. Kim, D.L. Carrol, Applied Physics Letters 87 (2005) 083506.
[2] D. Chen, A. Nakahara, D. Wei, D. Nordlund, T.P. Russell, Nano Letters 11 (2010) 561.
[3] W. Ma, C. Yang, X. Gong, K. Lee, A.J. Heeger, Advanced Functional Materials 15 (2005) 1617.
[4] M.T. Dang, L. Hirsch, G. Wantz, Advanced Materials 23 (2011) 3597.
[5] T. Ferenczi, J. Nelson, C. Belton, A.M. Ballantyne, M. Campoy-Quiles, F.M. Braun, D.D.C. Bradley, Journal of Physics: Condensed Matter 20 (2008) 475203.
[6] F.-C. Chen, C.-J. Ko, J.-L. Wu, W.-C. Chen, Solar Energy Materials and Solar Cells 94 (2010) 2426.
[7] N. Kim, I.H. Oh, S. Yoon, C.E. Lee, J.Y. Choi, B.H. Youn, C.Y. Jang, J. Kim, Journal of Korean Physics Society 55 (6) (2009) 2654.
[8] (a) H.-Y. Chen, H. Yang, G. Yang, S. Sista, R. Zadoyan, G. Li, Y. Yang, Journal of Physical Chemistry C 113 (2009) 7946;
(b) B. Peng, X. Guo, Y. Zou, C. Pan, Y. Li, Journal of Physics D: Applied Physics 44 (2011) 365101.
[9] A. Charas, Q. Ferreira, J. Farinhas, M. Matos, S. Fonseca, H. Burrows, L. Alcácer, J. Morgado, Macromolecules 42 (2009) 7903.
[10] J. Farinhas, Q. Ferreira, R.E. Di Paolo, L. Alcácer, J. Morgado, A. Charas, Journal of Materials Chemistry 21 (2011) 12511.
[11] K. Lu, Y. Guo, Y. Liu, C. Di, T. Li, Z. Wei, G. Yu, C. Du, S. Ye, Macromolecules 42 (2009) 3222.
[12] S. Miyanishi, K. Tajima, K. Hashimoto, Macromolecules 42 (2009) 1610.
[13] C. Yang, S. Holdcroft, Synthetic Metals 84 (1997) 563.
[14] B.J. Kim, Y. Miyamoto, B. Ma, J.M.J. Fréchet, Advanced Functional Materials 19 (2009) 2273.
[15] R.S. Loewe, P.C. Ewbank, J. Liu, L. Zhai, R.D. McCullough, Macromolecules 34 (2001) 4324.
[16] J. Pommerehne, H. Vestweber, W. Guss, R.F. Mahrt, H. Bassler, M. Porsch, J. Daub, Advanced Materials 7 (1995) 551.
[17] M. Trznadel, A. Pron, M. Zagorska, R. Chrzaszcz, J. Pielichowski, Macromolecules 31 (1998) 5051.
[18] A. Charas, L. Alcácer, A. Pimentel, J.P. Conde, J. Morgado, Chemical Physics Letters 455 (2008) 189.
[19] C.J. Brabec, A. Cravino, D. Meissner, N.S. Sariciftci, T. Fromherz, M.T. Rispens, L. Shanchez, J.C. Hummelen, Advanced Functional Materials 11 (2001) 374.
[20] A.G. Umnov, O.J. Korovyanko, Applied Physics Letters 87 (2004) 113506.
[21] A. Gadisa, M. Svensson, M. Anderson, O. Inganas, Applied Physics Letters 84 (2004) 1609.
[22] C.D. Müller, A. Falcou, N. Reckefuss, M. Rojahn, V. Wiederhirn, P. Rudati, H. Frohne, O. Nuyken, H. Becker, K. Meerholz, Nature 421 (2003) 829.
[23] M.-S. Kim, J.-S. Kim, J.C. Cho, M. Shtein, L.J. Guo, J. Kim, Applied Physics Letters 90 (2007) 123113.
[24] D.M. Nandith, M. Dissanayake, A.A.D.T. Adikaari, R.J. Curry, R.A. Hatton, S.R.P. Silva, Applied Physics Letters 90 (2007) 253502.
[25] W.-H. Baek, T.-S. Yoon, H. Ho Lee, Y.-S. Kim, Organic Electronics 11 (2010) 933.